Elucidating the role of hyaluronic acid in the structure and morphology of calcium oxalate crystals

Polat, Sevgi; Burak Eral, Huseyin

DOI
10.1016/j.apt.2021.08.021

Publication date
2021

Document Version
Final published version

Published in
Advanced Powder Technology

Advanced Powder Technology 32 (2021) 3650–3659

Contents lists available at ScienceDirect

Advanced Powder Technology

journal homepage: www.elsevier.com/locate/apt

Original Research Paper

Elucidating the role of hyaluronic acid in the structure and morphology of calcium oxalate crystals

Sevgi Polat [a,*], Huseyin Burak Eral [b,c]

[a] Department of Chemical Engineering, Faculty of Engineering, Marmara University, 34722 İstanbul, Turkey
[b] Van't Hoff Laboratory for Physical and Colloid Chemistry, Debye Institute for Nanomaterials Science, Utrecht University, 3584 CH Utrecht, the Netherlands
[c] Process & Energy Department, Delft University of Technology, 2628 CB Delft, the Netherlands

ARTICLE INFO

Article history:
Received 25 May 2021
Received in revised form 28 July 2021
Accepted 11 August 2021
Available online 25 August 2021

Keywords:
Calcium oxalate
Crystallization
Hyaluronic acid
Morphology
Kinetics

ABSTRACT

Recent surge in reports describing new additives that inhibiting the growth and nucleation of calcium oxalate (CaOx), the most common component of renal calculi or kidney stones, have rekindled interest in CaOx crystallization. In this in vitro study, the effect of hyaluronic acid (HA), a protein commonly found in urine, on the morphology and phase of the CaOx crystals is investigated. CaOx crystals were crystallized at pH 5.8 and 37 °C with a $[Ca^{2+}]$:$[C_2O_4^{2-}]$ ratio of 20:1, which is close to physiological conditions, in aqueous solution and artificial urine media. The obtained crystals were characterized structurally, morphologically and in terms of their surface charge. The crystals precipitated in aqueous solution without the HA additive were pure phase calcium oxalate monohydrate (COM) crystals with typical hexagonal morphology. The addition of HA partially promotes the transformation of COM into calcium oxalate dihydrate (COD) in aqueous solution. However, the only solid phase to form in artificial urine media with and without HA was identified as COD with tetragonal bipyramidal morphology. The results of this investigation will contribute to the understanding of the role HA plays on the morphology, structure, and thermal characteristics of CaOx and ultimately facilitate the development of effective treatments for kidney stones.

1. Introduction

Kidney stones are a widespread problem, with a increasing prevalence of 8–15% in general population [1,2]. The formation of kidney stones is complex phenomena and involves nucleation, crystal growth, crystal aggregation, and finally adhesion to the urinary tract lining. Kidney stones can be caused by various factors, including diet, the environment, genetics, and urinary infections [3–5]. Typically, kidney stones are formed from calcium oxalate (CaOx), hydroxyapatite, magnesium ammonium phosphate, uric acid, or cystine, with CaOx crystals found in approximately 80% of kidney stones [6–8]. CaOx takes three crystal forms: calcium oxalate monohydrate (COM, $CaC_2O_4{\cdot}H_2O$), calcium oxalate dihydrate (COD, $CaC_2O_4{\cdot}2H_2O$), and, rarely, calcium oxalate trihydrate (COT, $CaC_2O_4{\cdot}3H_2O$). COM is the most thermodynamically stable, whilst COD and COT are metastable phases. All three phases can be found within human urinary stones [9–12]. Moreover, the COM crystal form has high affinity for renal tubular cells, making it a significant contributor to urolithiasis pathogenesis [13]. The COD form is often present in the urine of healthy subjects while COM calculi are more prevalent in the urine of recurrent stone formers compared with urine from healthy subjects [14,15]. Thus, recent reports focused on how natural and synthetic additives, for example, amino acids [16–19], polymers [20,21], lipids [22], proteins [23,24], peptides [25,26], metal ions [27–29], and carboxylic acids [30,31], affect the formation of the different forms of CaOx and how they can be leveraged to prevent or treat kidney stones. Various additives show specific binding with different surfaces of the CaOx crystals and can inhibit their growth via various mechanisms [32]. Very low levels of these additives can have a dramatic effect on the structure and morphology of CaOx crystals [25]. In the present study, we focus on hyaluronic acid (HA), a commonly found protein in urine. Despite long standing suspicions on possible role on overexpressed HA, due to long term hydrodynamic stress or impact of stone fragments, influencing kidney stone formation. To date, the relationship between CaOx and HA was investigated from different points of view [33–36]. However, an in-vito study focusing on HA as a nucleation and growth modifier has not been fully reported in literature, to best of our knowledge.

* Corresponding author.
E-mail address: sevgi.polat@marmara.edu.tr (S. Polat).

https://doi.org/10.1016/j.apt.2021.08.021

Investigating the effect of HA on the crystallization of CaOx may shed light on how this additive may be used in the body to regulate CaOx crystallization. Thus, in this work, we systematically studied the effect of HA concentration on the structure, size, and morphology of the CaOx crystals precipitating in vitro. Furthermore, this work contributes to a improved understanding of the thermal characteristics, kinetics, and thermodynamics of sparsely soluble salts such as CaOx using coupled TGA/FTIR system. The model-free methods (FWO [37,38], KAS [39,40], Starink [41], and Tang [42]) were used to calculate the dehydration kinetic parameters of the COM crystals. Moreover, thermodynamics evaluation was performed in terms of calculating the enthalpy (ΔH), entropy (ΔS), and Gibbs free energy (ΔG) values. Finally, the main evolved gas products were observed using combined TGA/FTIR. Our results showed the use of HA as additive had a beneficial effect on the CaOx crystals by changing their morphology and reducing their size. We hope that the results reported here will conribute not only to development of preventive treatments that inhibit crystal formation in the urinary tract but also to broader biomineralization research.

2. Materials and methods

2.1. Materials

The calcium chloride dihydrate ($CaCl_2{\cdot}2H_2O$, ≥99.0%) and sodium oxalate ($Na_2C_2O_4$, ≥99.9%) were of analytical grade and were purchased from Merck (Darmstadt, Germany). Hyaluronic acid (CAS number 9067–32-7) employed as an additive was obtained from Sigma Aldrich (Gillingham, UK) and used as received without further purification. Deionized water was used to prepare the solutions.

2.2. Experimental methods

The crystallization of CaOx as a result of the reaction between $CaCl_2{\cdot}2H_2O$ (0.1 M) and $Na_2C_2O_4$ (0.005 M) was performed in batch crystallization mode in a cylindrical glass crystallizer with an active volume of 500 mL. The crystallizer was equipped with a thermostatic jacket, a mechanical stirrer, and a pH control system. A stirring mechanism comprised a three-blade propeller and mechanical mixer. CaOx crystals were synthesized at pH 5.8, 37 °C, and 400 rpm with a $[Ca^{2+}]$:$[C_2O_4^{2-}]$ ratio of 20:1 in aqueous solution and artificial urine media. Since the concentration of urinary calcium ions in normal humans is 10–20 times that of urinary oxalate, the ratio of $[Ca^{2+}]$:$[C_2O_4^{2-}]$ was selected as 20:1 [19,43]. The artificial urine was prepared using the method described in a previous study [43,44] and its content was as follows: 0.01695 M Na_2SO_4, 0.00385 M $MgSO_4{\cdot}7H_2O$, 0.0455 M NH_4Cl, 0.0637 M KCl, 0.1055 M NaCl, 0.0323 M NaH_2PO_4, and 0.00321 M $Na_3C_6H_5O_7$.

For the synthesis of CaOx crystals, 250 mL of $Na_2C_2O_4$ solution was added to the crystallizer containing 250 mL of $CaCl_2$ solution at a rate of 5 mL/min by means of a peristaltic pump. Once all of the reactants had been added to the crystallizer, the suspension was allowed to mix for 1 h at the desired temperature (37 ± 0.1 °C). The suspension was then filtered through a 0.45-μm membrane filter (Millipore) and the obtained crystals were washed with deionized water and ethanol, then left to dry at room temperature. The dried crystal samples were then used for the subsequent analyses. HA at concentrations varying between 0 and 1 mM was added to the $CaCl_2$ solution prior to the addition of the $Na_2C_2O_4$ solution in order to investigate the effects of HA as an additive on the crystallization process.

2.3. Characterization

The X-ray diffraction (XRD) was performed using a Bruker D2 Phaser Tabletop Diffractometer with Cu Kα radiation (λ = 1.5418 Å) at a scanning rate of 4°/min in the 2θ range from 10° to 70° for phase identification. Fourier-transform infrared spectroscopy (FTIR) analysis was carried out using a Shimadzu IR Affinity-1 equipped with ATR accessories. Measurements were performed at room temperature between 600 and 4000 cm^{-1} in transmission mode with a resolution of 4 cm^{-1} with eight scans per sample. The morphology of CaOx crystals were examined using scanning electron microscopy (SEM, Zeiss EVO LS 10) with an accelerating voltage of 15 kV. The atomic force microscopy (AFM) was also used to characterize the morphology of the samples. The analysis was performed using Shimadzu SPM-9600 operating in tapping mode with the scan frequency of 0.5 Hz. All the images were taken in constant force mode at scan area 10 × 10 μm^2 and collected at 256 × 256-pixel resolution. The zeta potential (ζ potential) of the crystalline product was analyzed by the Zeta Sizer Nano Series Nano-ZS (Malvern). Each measurement was repeated at least 10 times, and the average value was calculated. All experiments were performed at 25 °C and pH 5.8. The thermal degradation behavior of the crystals and the crystal water content in the solid samples were determined using the SDT Q600 thermogravimetric analyzer (TA Instruments) by scanning the temperature range from 25 to 1000 °C at a heating rate of 20 °C/min. Before each thermal analysis, a blank experiment was performed to obtain the baselines to eliminate the systematic errors of the instrument. A continuous high purity nitrogen (99.999%) with a flow rate of 30 mL/min was supplied to maintain an inert atmosphere. To ensure maximum accuracy and to minimize errors, all experiments were conducted at least as triplicates. In order to calculate the dehydration kinetics and thermodynamic parameters of COM crystals, thermogravimetric analysis (TGA) was performed at different heating rates of 5, 10, and 20 °C/min. The data collected were further analyzed by aforementioned models for kinetic analysis. The information for the thermo-kinetic models, their equations, and the plotting methods (Table S1) is provided in Supporting Information (SI). The simultaneous evolution of the gases during thermal decomposition was detected using the Tensor27 FTIR (Bruker) combined with TGA with a heating rate of 20 °C/min. The transfer line from TGA to FTIR was kept at 200 °C to avoid gas condensation. The FTIR spectra were recorded from 4000 to 400 cm^{-1} at a resolution of 4 cm^{-1}.

3. Results and discussion

3.1. XRD and FTIR analyses

Fig. 1a shows the XRD patterns of the CaOx crystals obtained in aqueous solution and artificial urine media with and without the addition of HA. The XRD results showed that different types and amounts of CaOx crystals were obtained in aqueous solution with and without HA. The CaOx crystals obtained in aqueous solution without HA were in the form of monoclinic COM structure and no other forms were detected. In agreement with Joint Committee on Powder Diffraction Standards [JCPDS]: 00–020-0231, the main diffraction peaks for CaOx crystals prepared without HA were located at 2θ of 14.94, 24.52, 30.22, 36.14, and 38.18°, which are assigned to the (101), (020), ($\bar{2}$02), (112), and (130) planes, respectively of COM crystals with space group $P2_1/c$. Similar peaks were also detected for CaOx crystals obtained in the presence of a low HA concentration (0.05 mM) and the crystallized product was in COM form, as in aqueous solution. In other words, a low additive concentration has no detectable effect on the crystalline structure and hydrates within the resolution of PXRD. However, at HA

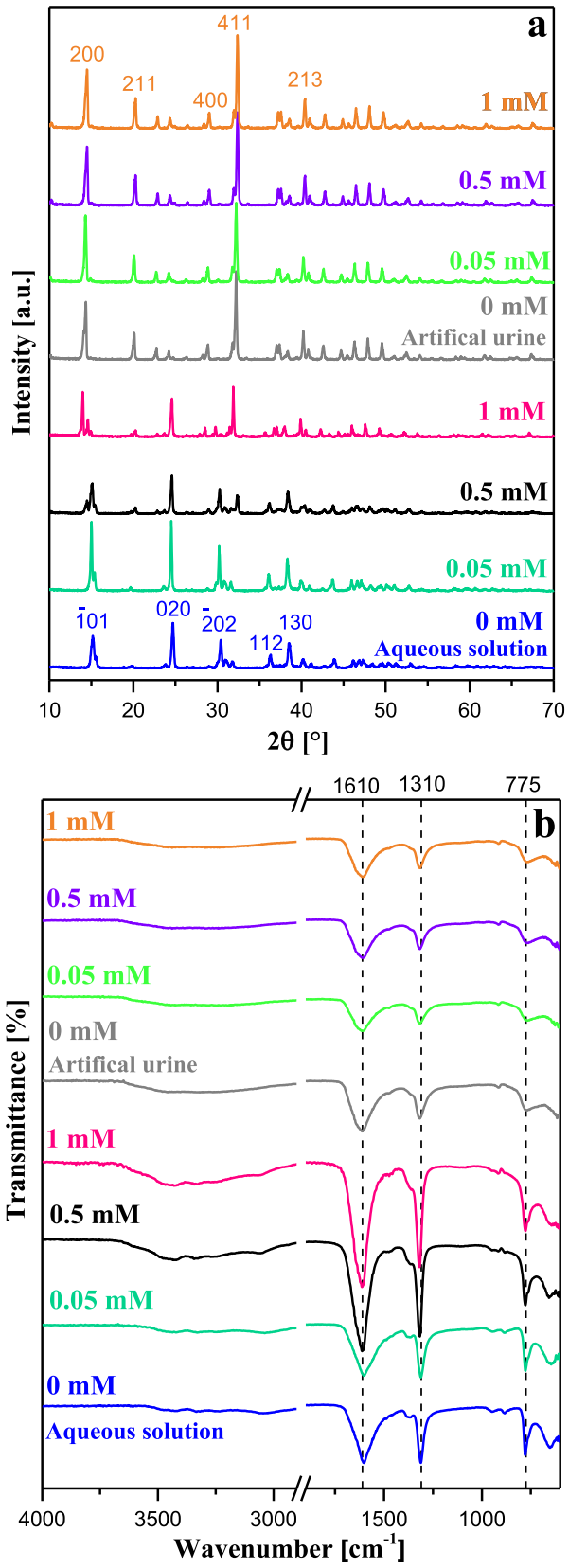

Fig. 1. a) XRD results and b) FTIR results for the calcium oxalate (CaOx) crystals synthesized in aqueous solution and artificial urine media with different concentrations of hyaluronic acid (HA).

concentrations of 0.5 mM and 1 mM, low-intensity peaks characterizing the COD form as well as COM hydrate were detected. In addition to main the reflection of COM crystals, the new reflections were observed at 14.34, 20.08, 28.88, 32.22, and 40.20°, which were assigned to the (200), (211), (400), (411), and (213) planes of COD crystals (JCPDS: 00–017-0541), respectively. This result revealed that a fraction of COM crystals was transformed into the COD form and this deduction was confirmed by FTIR analysis. As shown in FTIR spectra in Fig. 1b, the five absorption peaks between 3510 and 2950 cm^{-1} were associated with the water O–H stretching vibrations for the crystalline products obtained in aqueous solution without HA. Moreover, the C – O stretching, C – C stretching, and O – C – O plane bending vibrations were assigned to the absorption peaks at ~ 950 cm^{-1}, 880 cm^{-1}, and 660 cm^{-1}, respectively [45–47]. At higher HA concentrations, the intensities of the COM peaks decreased slightly, and new specific COD peaks were detected. In addition, slight shifts from 1605 and 1310 cm^{-1} towards 1610 and 1316 cm^{-1}, respectively, were observed. This shift indicated that some COM crystals, albeit a small amount, were converted into the COD form. The proportion of COM gradually decreased while that of COD gradually increased, thus consistently supported the corresponding XRD results. There were also five peaks for CaOx crystals within the range of ~ 3600–2900 cm^{-1} for the COM form. For the COD crystals, these five peaks were replaced by a single wide peak. When the peaks in this range were examined, while the five COM peaks were more prominent in crystals prepared in aqueous solution without HA, this prominence was slightly reduced with HA concentrations of 0.5 mM and 1 mM. In other words, with increasing HA concentration the five peaks merged to give a single peak. When the XRD patterns for the crystalline product obtained in artificial urine media without HA were examined, the crystals only exhibited tetragonal COD crystal structure with space group *I*4/*m*. Adding the HA to the crystallization medium did not change the phase composition and the crystals maintained the COD form, which was supported by the FTIR results, however, the changes in the peak intensities of the crystals and shifting were observed for some diffraction peaks. These changes could result from the incorporation of the additive molecules within the crystal lattice. In this circumstance, structural imperfections and internal strains occur in the individual lattice symmetry. As a result of this, the shifting and changing in peaks occur in the presence of HA compared to those in the pure media.

3.2. SEM analysis

SEM analysis was performed to determine whether the HA influenced CaOx crystal size and morphology. Fig. 2 shows the SEM images of the CaOx crystals synthesized in aqueous solution with various HA concentrations. The CaOx crystals not containing HA were composed of hexagonal COM crystals which was consistent with the results of previous studies [32,45,48,49]. In addition, it consisted of compact aggregates as a result of the growth of COM crystals on other COM crystals and the main growth of the crystal was on the ($\bar{1}$01) face. The morphology of the COM crystals prepared in aqueous media containing 0.05 mM HA changed considerably and they started to lose their hexagonal appearance. Although the resulting crystals had generally curved edges, large amounts of pairs of crystals were formed and the crystals formed tend to grow in a stratified manner independently of their forms. Compared to the crystals prepared in the absence of HA, the aggregation tendency was reduced considerably with the addition of HA, deformations on the crystal surfaces decreased, and the surfaces appeared smooth. The formed crystals showed a homogeneous appearance. The CaOx crystal morphology continued to change with the increase in the HA concentration to 0.5 mM. Both elliptical COM crystals and a small quantity of bipyramidal tetragonal COD crystals were formed. Compared to the crystals formed with 0.05 M HA, there was a decrease in the particle size. Similar to 0.5 mM

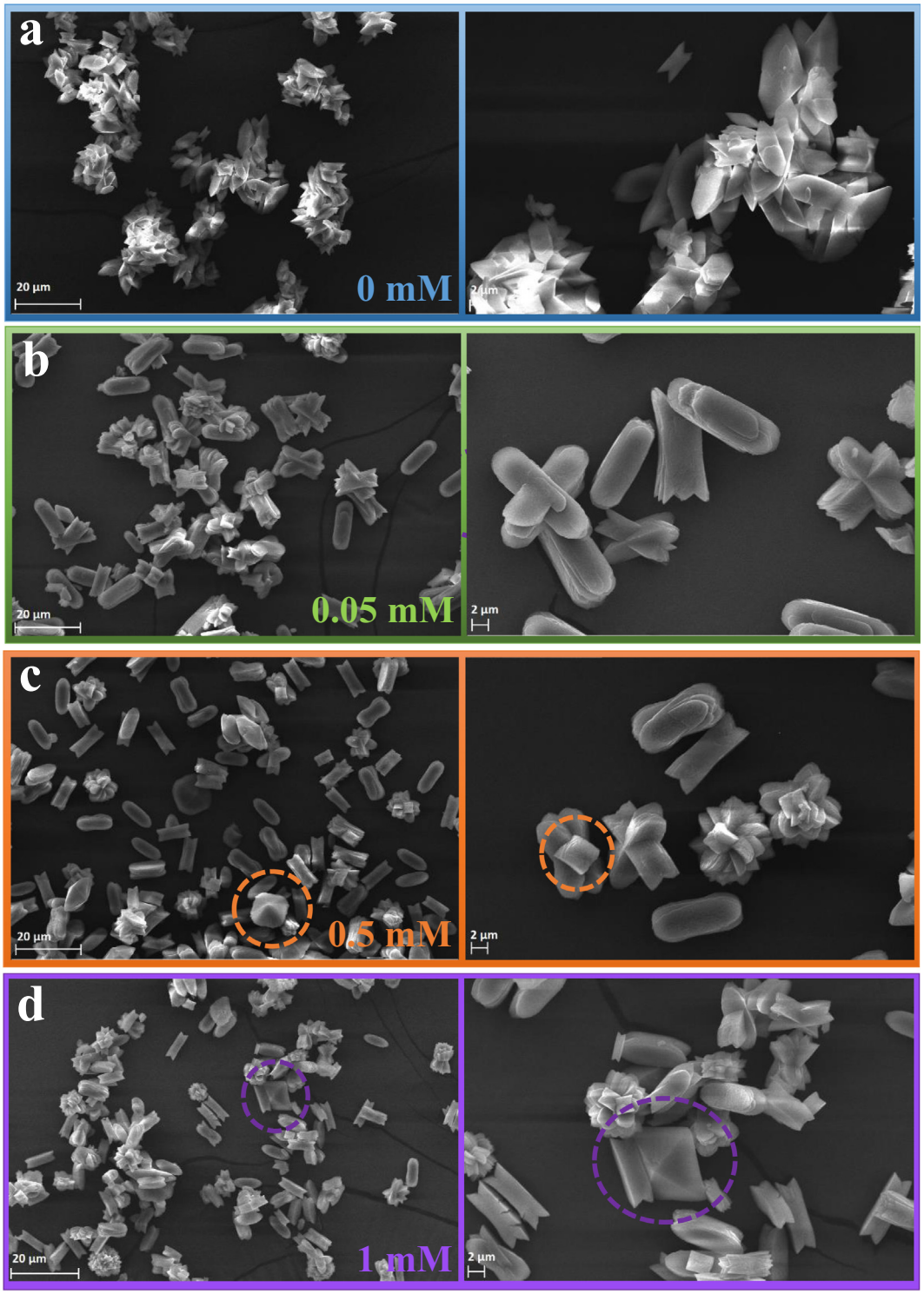

Fig. 2. SEM images of the calcium oxalate (CaOx) crystals synthesized in aqueous solution with different concentrations of hyaluronic acid (HA). a) 0 mM, b) 0.05 mM, c) 0.5 mM, d) 1 mM.

HA concentration, a small amount of well-surfaced bipyramidal COD crystals were formed at 1 mM additive concentration. The SEM results also supported the partial phase transformation from the COM form to the COD form at higher HA concentration. It seems likely that HA has an inhibitory effect on the growth of COM crystals, preventing their aggregation and thus promoting the formation of the COD form. Several hypotheses have been put forward to explain the mechanism through which modifiers affect COM crystallization. One suggestion is that impurities are adsorbed on the face of the crystals or enter the crystals, while another report proposed that the degree of hydration of COM leads to the formation of a metastable phase of COD [50,51]. The results of the current study suggest that HA has a slight impact on CaOx crystal size, while conversely the degree of aggregation of the crystals decreases with the addition of HA and some COD is formed. Yet we can conclusively relate the observed effect of decreasing

aggregation with increasing HA concentration solely on HA. Evaporation can also be partially responsible as SEM analysis requires dried crystals. In other words, sample preparation procedure for ex-situ SEM involving evaporation might also contribute to aggregation.

In addition to the crystals produced in aqueous solution, SEM analysis was also performed for the CaOx crystals obtained in artificial urine media to mimic physiological conditions and to better determine the effect of the HA additive. As shown in Fig. 3, CaOx crystals produced in artificial urine media without HA had smooth-surfaced homogeneously shaped bipyramidal COD crystals. Similar to with the aqueous solution media, the CaOx crystals grew on each other and compact aggregate structures were formed. In addition, growth disorders were detected on the crystal surface. The addition of 0.05 mM HA to the media had no significant effect on the crystal size or morphology. With the increase in the HA concentration to 0.5 mM, the crystal morphology maintained its tetragonal bipyramidal form, but the crystals showed a flatter shape, as shown in Fig. 3b. At the same time, the sharp edges of these crystals were rounded. With a HA concentration of 1 mM, the crystals were further flattened and the edges became even more round. At the same time, the aggregation tendency decreased, and the average particle size decreased by about 40%. The SEM images of the crystals suggest that supplementation of the media with HA changed the morphology of the obtained crystals, as well as reducing their particle size and tendency to agglomerate.

In addition to SEM analysis, the changes in the topography of the CaOx crystals obtained in artificial urine media with and without HA were also confirmed by AFM analysis. The results are given in Figure S1. The surface morphology and roughness of the CaOx crystals produced in artificial urine media without HA was variable with a maximum difference of 231.18 nm in thickness. This difference decreased with the addition of the HA to the media, which indicated a decrease surface roughness and irregularity.

Finally, it is worthwhile to discuss why only COD crystals were observed in the presence of HA in artificial urine while addition of HA resulted in partial transformation from COM to COD in deionized water. Despite the fact that same HA concentrations are used in experiments with deionized water and artificial urine, the solution chemistry is significantly different. Consequently, supersaturations where crystallization occurred in deionized water and artificial urine are different due to combined effect of ionic strength, protonation reactions, and soluble complex formation [49]. The complex solution chemistry of artificial urine solution may overshadow the form altering effect of HA observed in deionized water by increasing the supersaturation across all solutions. Alternatively, the solution chemistry of artificial urine may alter the conformations of HA altering how HA surface groups interacts with CaOx crystals. Yet without detailed solution chemistry modeling considering the role of HA in solution chemistry, which is beyond the scope of this study, underlying physical mechanism of aforementioned (pseudo) polymorphic transition remains an open question.

3.3. Zeta potential analysis

Zeta (ζ) potential analysis was applied to investigate the surface charge between the particles since this has a direct relationship with

Table 1
The zeta (ζ) potential of calcium oxalate (CaOx) crystals as a function of hyaluronic acid (HA) concentration.

Hyaluronic Acid (mM)	ζ potential in aqueous solution (mV)	ζ potential in artificial urine (mV)
0	−1.6 ± 0.80	−2.8 ± 0.36
0.05	−21.2 ± 1.54	−12.3 ± 1.92
0.5	−16.7 ± 1.66	−24.1 ± 2.74
1	−19.5 ± 1.71	−32.4 ± 2.93

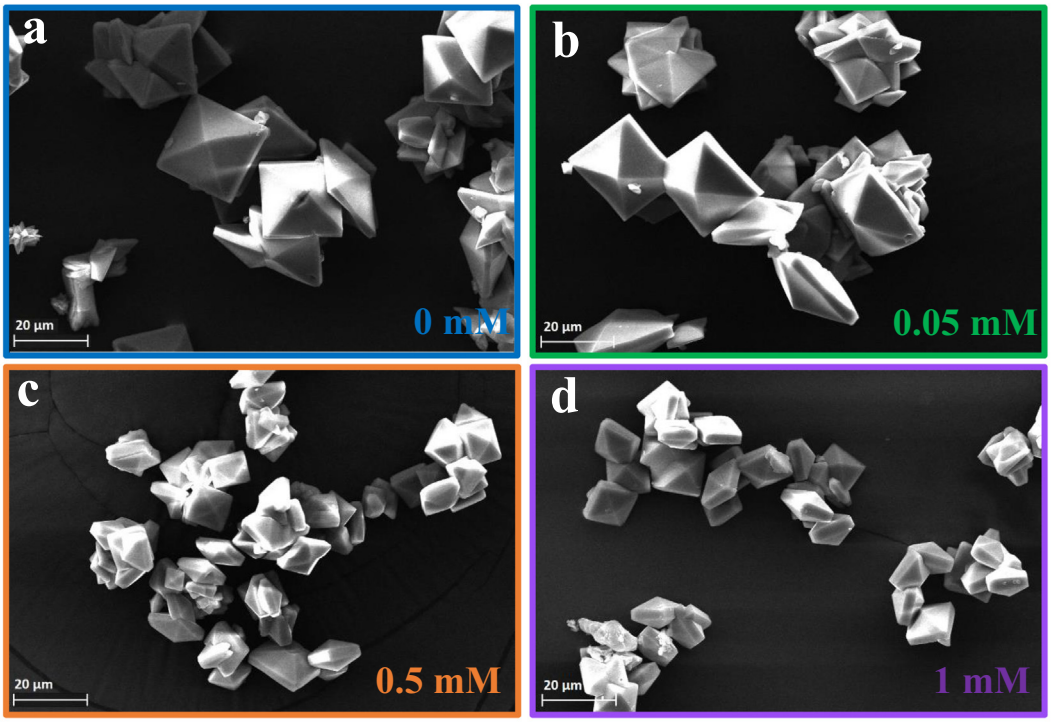

Fig. 3. SEM images of the calcium oxalate (CaOx) crystals synthesized in artificial urine with different concentrations of hyaluronic acid (HA). a) 0 mM, b) 0.05 mM, c) 0.5 mM, d) 1 mM.

crystal agglomeration. Particles with a high ζ cannot easily form aggregates because of their high electrostatic repulsion and stability, and vice versa [44]. The ζ potentials of the CaOx crystals obtained in aqueous solution and artificial urine media with different concentrations of HA are given in Table 1. The CaOx crystals obtained in aqueous solution and artificial urine media without the addition of HA had zeta potential of −1.6 ± 0.80 mV and −2.8 ± 0.36 mV, respectively. The ζ potential results indicated that the CaOx crystals obtained under all studied HA conditions exhibited a negatively charged surface. Increasing the HA concentration in the medium made the zeta potential more negative due to the crystal surface being covered with the negatively charged ions of HA.

The crystals produced in artificial urine media showed a similar trend in zeta potential results to the crystals prepared in aqueous solution. Compared to COM crystals, electrostatic repulsion between the COD crystals was larger so they could not easily aggregate to form stones. With increasing HA concentration, the absolute ζ potential value increased. Zeta potentials greater than + 30 mV or less than −30 mV normally indicate stable particles with a low propensity for aggregation [52]. With the absolute increase in the ζ potential value, the electrostatic repulsion increased, leading to crystals repelling each other, which could inhibit the aggregation of CaOx crystals. This result was also supported by SEM analysis. In both aqueous solution and artificial urine media, adding HA reduced the tendency for agglomeration, resulting in more stable crystals.

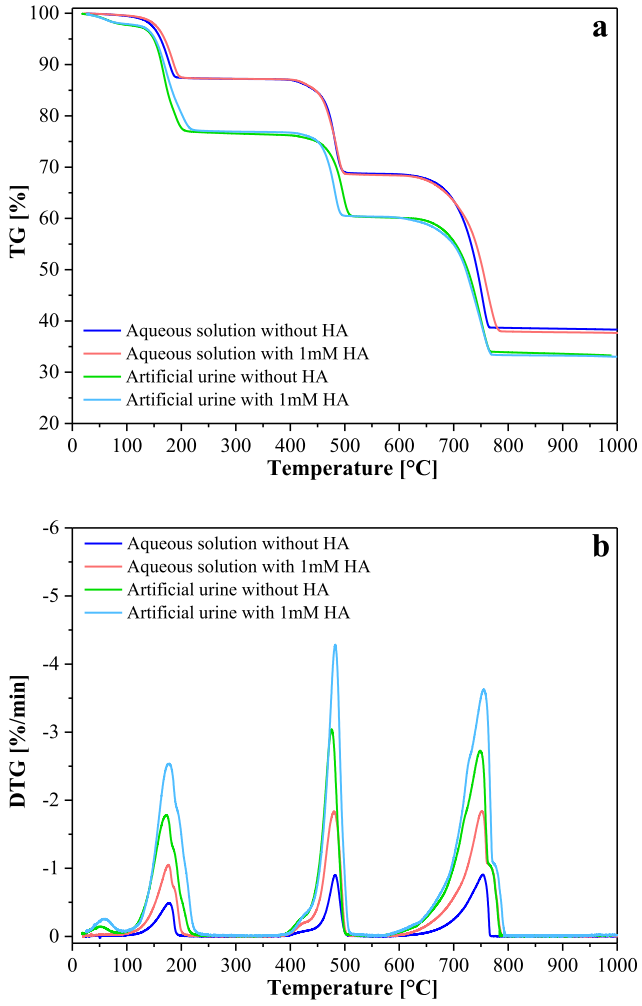

Fig. 4. a) TG and b) DTG curves for the calcium oxalate (CaOx) crystals synthesized in aqueous solution and artificial urine with and without hyaluronic acid (HA).

3.4. Tga/Ftir

The thermal degradation mechanism of CaOx crystals included three weight loss steps, as shown in the following equations [53–55]:

$$CaC_2O_4 \cdot xH_2O \rightarrow CaC_2O_4 + xH_2O \quad (1)$$

$$CaC_2O_4 \rightarrow CaCO_3 + CO \quad (2)$$

$$CaCO_3 \rightarrow CaO + CO_2 \quad (3)$$

Fig. 4 shows the degradation profiles of the crystals obtained with and without the addition of HA in aqueous solution and artificial urine media and the corresponding differential curve (DTG). The dehydration stage occurred at ~175 °C for the CaOx crystals obtained in aqueous solution, where the crystal water in the oxalates is removed, with an obvious weight loss of 12.2 %, which is close to the theoretical value for COM of 12.3%. At temperatures ranging from ~410 to 510 °C, the second weight loss of ~19.0 % was detected, which corresponded to the splitting of carbon monoxide. Finally, between ~650 and 760 °C, the calcium carbonate in the sample decomposed into calcium oxide with the loss of carbon dioxide and a weight loss of ~ 30.0%. The final residue obtained at the end of degradation was 38.5 wt%, which agreed with the theoretical value of the COM crystals. The crystals prepared in the presence of HA in aqueous solution exhibited a slight new peak in the temperature range of ~ 40–100 °C, indicating the partial phase transformation from COM to COD, in agreement with the XRD and FTIR results. As shown in Fig. 4, the COD crystals underwent dehydration at ~180 °C with a weight loss of ~ 22.0 %, close to the theoretical value of 21.95% for COD. The weight loss in the first dehydration stage for both TG curves further confirmed that the crystals grown in aqueous solution were COM while those prepared in artificial urine were COD.

Although TGA gathers important information about the thermal degradation behavior of the samples, identifying gaseous compounds that evolved during the thermal process is also valuable for gathering information on the degradation pathways; therefore, TGA/FTIR analysis was simultaneously performed to visualize the thermal degradation of the CaOx and determine the volatile species at corresponding wavenumbers in real time. The Gram–Schmidt (GS) profile derived from FTIR analysis indicated how the

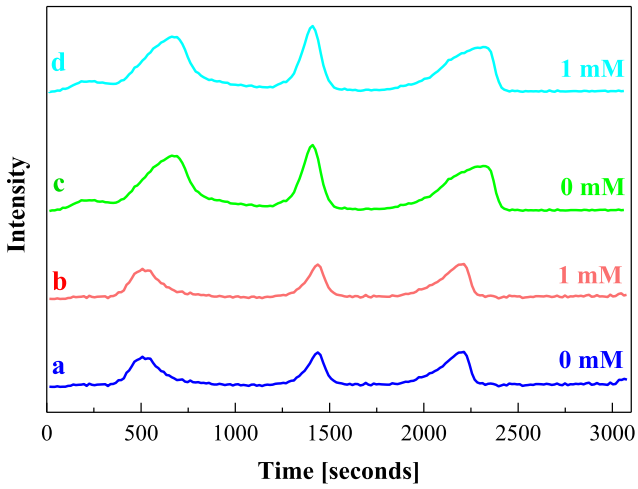

Fig. 5. Gram-Schmidt curves a) Calcium oxalate (CaOx) crystals synthesized in aqueous solution without hyaluronic acid (HA). b) CaOx crystals synthesized in aqueous solution with 1 mM HA. c) CaOx crystals synthesized in artificial urine without HA. d) CaOx crystals synthesized in artificial urine with 1 mM HA.

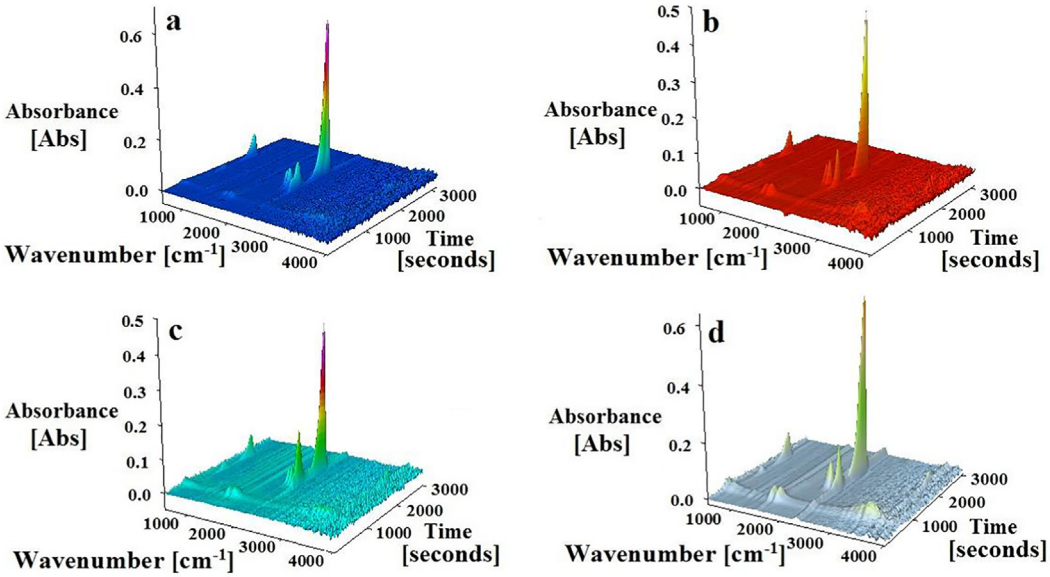

Fig. 6. Three-dimensional FTIR spectra. a) Calcium oxalate (CaOx) crystals synthesized in aqueous solution without hyaluronic acid (HA). b) CaOx crystals synthesized in aqueous solution with 1 mM HA. c) CaOx crystals synthesized in artificial urine without HA. d) CaOx crystals synthesized in artificial urine with 1 mM HA.

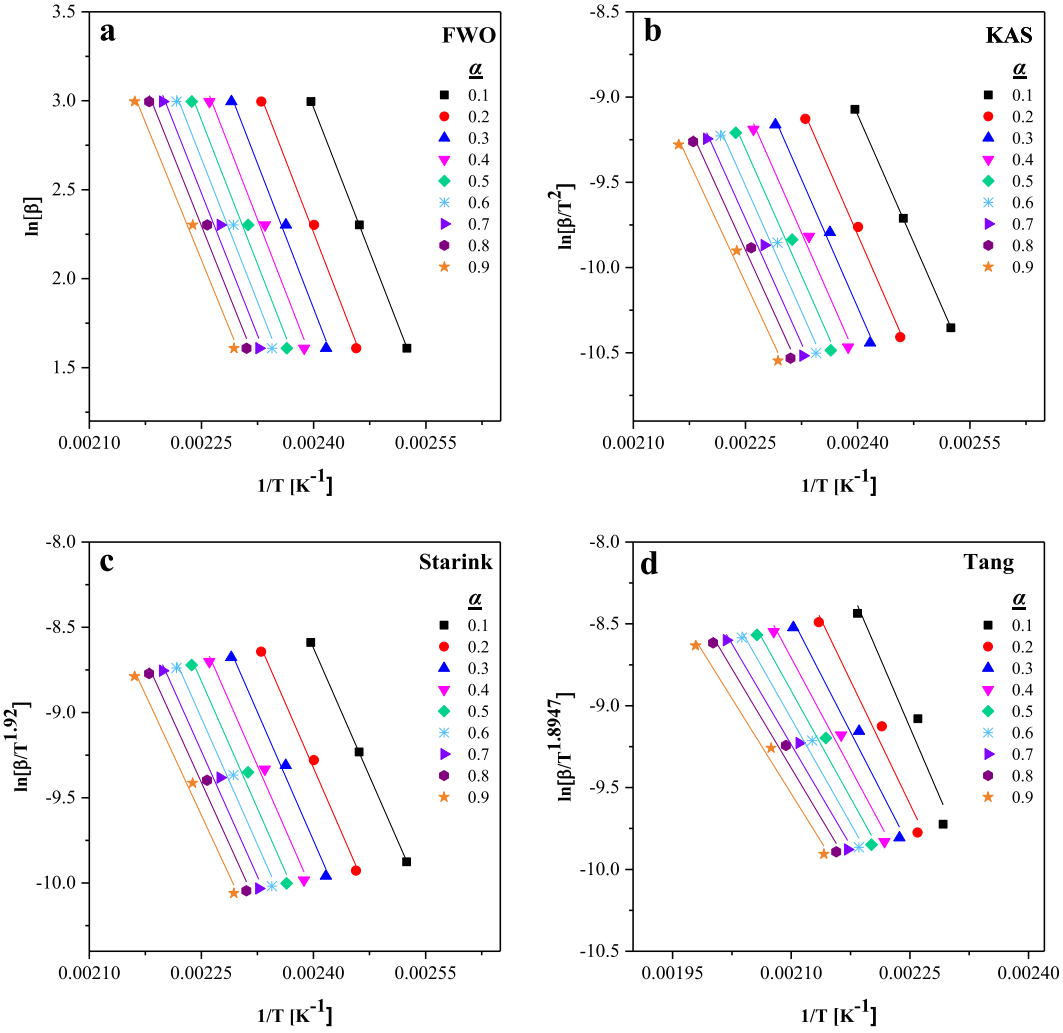

Fig. 7. Plots of a) FWO, b) KAS, c) Starink, and d) Tang models for calcium oxalate monohydrate (COM).

concentration of the evolved gases varied during the thermal decomposition process. These GS profiles for the crystals obtained with and without the addition of HA in aqueous solution and artificial urine media are presented in Fig. 5. These GS profiles directly correlated with the stages in the TGA curves. When we compared these to the DTG curves, we observed that only the peak temperature in the GS curve shifted slightly toward the higher region, which was the result of the short time delay in the transport of the evolved volatiles from TGA to FTIR. H_2O, CO, and CO_2 were identified as the gaseous species released during the thermal degradation of CaOx crystals and their 3-dimentional (3D) FTIR spectra are illustrated in Fig. 6. The characteristic bands located in the 3000–3500 cm cm^{-1} region show the O–H stretching vibration related to the water molecules. Comparing the 3D FTIR spectra for the crystals prepared in aqueous solution and artificial urine, the absorption intensity of the O–H stretching vibration was higher for the crystals prepared in artificial urine, confirming that the COD form was formed. The absorption bands at about 2100 cm^{-1} indicated the existence of CO. The bands at about 670 and 2350 cm^{-1} are the characteristic peaks of CO_2.

3.5. Kinetic and thermodynamic analysis

Thermal analysis has been used to study the kinetics of formation of COM, most thermodynamically stable and the primary crystal within pathogenic stones, to mimic what is occurring in renal stones. In the present study, the dehydration kinetics and thermodynamic parameters of COM crystals were calculated by using four common isoconversional kinetic methods, namely the Flynn–Wall–Ozawa (FWO) [37,38], Kissinger–Akahira–Sunose (KAS) [39,40], Starink [41], and Tang [42] models. Figure S2 illustrates the TG and DTG curves of the COM crystals obtained at three different heating rates in the dehydration zone, which was taken into consideration to calculate the activation energy. Moreover, Table S2 summarizes the characteristic dehydration temperatures, such as the initial temperature (T_i), peak temperature (T_{peak}), and final temperature (T_f). The same dehydration trend was detected for all studied heating rates for COM crystals. The dehydration temperatures shifted to the high temperature as heating rates increased resulting from an increase in subsequent thermal lag.

The activation energy, representing the minimum energy requirement, was calculated from the slopes of the lines derived from the FWO, KAS, Starink, and Tang models within a range of α = 0.1–0.9 in increments of 0.1. The plots are illustrated in Fig. 7. As seen in Fig. 7, the individual lines are nearly parallel for all four models, and there was a good fit between each model and its experimental data. Table 2 and Figure S3 demonstrate how the activation energy obtained from isoconversional models is dependent on the extent of conversion. The R^2 values of all lines were > 0.950, which indicated the reliability and accuracy of the results. The calculated activation energy was within the range of 78.3–86.0 kJ/mol and the mean values were 84.6 ± 3.03, 81.8 ± 3.67, 82.0 ± 3.64, and 82.1 ± 3.64 kJ/mol using the FWO, KAS, Starink, and Tang models, respectively. These calculated values were consistent with the reported activation energies in previous studies [56–58]. Masuda et al. [56] and Vyazovkin [57] calculated the variances in activation energy for the dehydration step were 77.5–86.0 kJ/mol and 75–105 kJ/mol, respectively. Chunxiu et al. [58] estimated that the activation energies for the dehydration process of COM crystals varied from 76.58 to 83.03 kJ/mol and 79.14 to 85.19 kJ/mol with average of 78.34 kJ/mol, and 81.33 kJ/mol by KAS and FWO models, respectively.

When the results of pre-exponential factors were examined, some variations based on the degree of conversion were detected. These values changed from 7.98 × 10^8/min to 6.72 × 10^9/min (Table 3). Based on the obtained activation energy and pre-exponential factor, the thermodynamic parameters, such as ΔH, ΔS, and ΔG, were further calculated using Eyring equations [59,60] during the thermal degradation of COM crystals. Table 3 presents the values of thermodynamic parameters for COM

Table 2
Activation energies (E, kJ/mol) with respect to conversion degrees for thermal degradation of calcium oxalate monohydrate (COM) crystals.

Conversion α	FWO		KAS		Starink		Tang	
	E	R^2	E	R^2	E	R^2	E	R^2
0.1	85.4	0.9999	83.1	0.9999	83.3	0.9999	83.3	0.9994
0.2	86.0	0.9960	83.6	0.9952	83.8	0.9853	83.8	0.9910
0.3	85.9	0.9925	83.2	0.9910	83.5	0.9911	83.5	0.9924
0.4	85.6	0.9902	82.9	0.9883	83.1	0.9884	83.1	0.9893
0.5	85.2	0.9885	82.4	0.9863	82.6	0.9865	82.7	0.9864
0.6	84.8	0.9875	81.9	0.9850	82.1	0.9852	82.1	0.9860
0.7	84.1	0.9872	81.1	0.9847	81.3	0.9848	81.4	0.9999
0.8	83.1	0.9880	80.0	0.9855	80.2	0.9856	80.2	0.9857
0.9	81.5	0.9903	78.3	0.9875	78.5	0.9883	78.6	0.9885
Average	84.6 ± 3.03		81.8 ± 3.67		82.0 ± 3.64		82.1 ± 3.64	

Table 3
Thermodynamic parameters for thermal degradation of calcium oxalate monohydrate (COM) crystals at 20 °C/min.

α	FWO				KAS				Starink				Tang			
	A	ΔH	ΔG	ΔS	A	ΔH	ΔG	ΔS	A	ΔH	ΔG	ΔS	A	ΔH	ΔG	ΔS
0.1	5.66 × 10^9	81.6	113.7	−70.1	2.99 × 10^9	79.3	113.8	−75.4	3.16 × 10^9	79.5	113.7	−74.9	3.19 × 10^9	79.5	113.7	−74.8
0.2	6.72 × 10^9	82.2	113.6	−68.7	3.40 × 10^9	79.8	113.7	−74.3	3.60 × 10^9	80.0	113.7	−73.8	3.63 × 10^9	80.0	113.7	−73.7
0.3	6.38 × 10^9	82.1	113.7	−69.1	3.12 × 10^9	79.5	113.7	−75.0	3.31 × 10^9	79.7	113.7	−74.5	3.34 × 10^9	79.7	113.7	−74.4
0.4	5.91 × 10^9	81.8	113.7	−69.8	2.81 × 10^9	79.1	113.8	−75.9	2.98 × 10^9	79.3	113.8	−75.4	3.01 × 10^9	79.3	113.7	−75.3
0.5	5.36 × 10^9	81.4	113.7	−70.6	2.48 × 10^9	78.6	113.8	−77.0	2.63 × 10^9	78.8	113.8	−76.4	2.66 × 10^9	78.9	113.7	−76.3
0.6	4.73 × 10^9	81.0	113.7	−71.6	2.13 × 10^9	78.1	113.8	−78.2	2.27 × 10^9	78.3	113.8	−77.7	2.29 × 10^9	78.3	113.8	−77.5
0.7	3.92 × 10^9	80.3	113.8	−73.2	1.72 × 10^9	77.3	113.8	−79.9	1.84 × 10^9	77.5	113.8	−79.4	1.86 × 10^9	77.6	113.8	−79.3
0.8	2.97 × 10^9	79.3	113.8	−75.5	1.26 × 10^9	76.2	113.9	−82.5	1.35 × 10^9	76.4	113.9	−82.0	1.36 × 10^9	76.4	113.9	−81.8
0.9	1.95 × 10^9	77.7	113.9	−79.0	7.98 × 10^8	74.5	114.0	−86.4	8.52 × 10^8	74.7	114.0	−85.8	8.61 × 10^8	74.8	113.9	−85.6
Av.	4.54 × 10^9	80.8	113.7	−72.0	2.30 × 10^9	78.0	113.8	−78.3	2.44 × 10^9	78.2	113.8	−77.8	2.47 × 10^9	78.3	113.8	−77.6

crystals at 20 °C/min. Figures S4-S7 show the results of pre-exponential factors and the thermodynamic parameters at each conversion level for FWO, KAS, Starink, and Tang models for three different heating rates. The ΔH varied between 82.2 and 74.5 kJ/mol with the average values being 80.8, 78.0, 78.2, and 78.3 kJ/mol for the FWO, KAS, Starink, and Tang models at 20 °C/min, respectively. The positive values of ΔH proved that the dehydration process was endothermic. The ΔS was between − 68.7 and − 86.4 J/mol K, and ΔG was within the range of 113.6–114.0 kJ/mol.

4. Conclusion

This study focused on how the presence of HA influences the crystal structure and morphology of CaOx crystals in aqueous solution and artificial urine. The XRD and FTIR results demonstrated that the CaOx crystals prepared in aqueous solution were mainly COM form, while the COD form was predominantly formed in artificial urine. In the aqueous solution, at higher HA concentrations (0.5 mM and 1 mM), CaOx was present in both COM and COD forms together, showing partial phase transformation from COM to COD. Presence of HA made measured zeta potential more negative as a result of the adsorption of additive onto the CaOx crystals. SEM images revealed that increasing concentrations of HA significantly altered the CaOx morphology and reduced the size of the crystals. The TGA/FTIR results showed that the CaOx crystals decomposed in three steps, with the main evolved gases being H_2O, CO, and CO_2. The results of kinetics analysis by FWO, KAS, Starink, and Tang models demonstrated that the activation energy value varied between 78.3 and 86.0 kJ/mol. Based on thermodynamic parameter, it was detected that the dehydration process was endothermic due to the positive enthalpy values. The results obtained in this study highlight the effects of HA on the form of CaOx produced, as well the particle size and morphology. In the future, the outcomes of this physiochemical study may guide the development of novel treatments that favor the formation of the thermodynamically less stable COD, which is less likely to form stones in the kidneys.

Declaration of Competing Interest

The authors declare that they have no known competing financial interests or personal relationships that could have appeared to influence the work reported in this paper.

Appendix A. Supplementary data

Supplementary data to this article can be found online at https://doi.org/10.1016/j.apt.2021.08.021.

References

[1] V. Romero, H. Akpinar, D.G. Assimos, Kidney Stones: A global picture of prevalence, incidence, and associated risk factors, Rev. Urol. 12 (2010) e86–e96.
[2] M.H. Lin, Y.L. Song, P.A. Lo, C.Y. Hsu, A.T.L. Lin, E.Y.H. Huang, H.K. Chiang, Quantitative analysis of calcium oxalate hydrate urinary stones using FTIR and 950/912 cm^{-1} peak ratio, Vib. Spectrosc. 102 (2019) 85–90.
[3] M.A. Boim, I.P. Heilberg, N. Schor, Phyllanthus niruri as a promising alternative treatment for nephrolithiasis, Int. Braz. J. Urol. 36 (6) (2010) 657–664.
[4] Ê.R. Dias, T. de L.M. Freire Dias, M.S. Alexandre-Moreira, A. Branco, Flavonoid-rich fraction from Pleroma pereirae (Melastomataceae): Effects on calcium oxalate crystallization, antioxidant and antinociceptive activities, Eur. J. Integr. Med. 35 (2020) 101095.
[5] F.L. Coe, A. Evan, E. Worcester, Kidney stone disease, J. Clin. Invest. 115 (2005) 2598–2608.
[6] S.R. Khan, M.S. Pearle, W.G. Robertson, G. Gambaro, B.K. Canales, S. Doizi, O. Traxer, H. Tiselius, Kidney stones. Nat. Rev. Dis. Primers. 25 (2) (2016) 16008.
[7] J. Zhang, L. Wang, W. Zhang, C.V. Putnis, Role of hyperoxaluria/hypercalciuria in controlling the hydrate phase selection of pathological calcium oxalate mineralization, Cryst. Growth Des. 21 (2021) 683–691.
[8] O. Bottrill, M. Boon, T. Barker, F. Jones, Calcium oxalate crystallization in synthetic urinary medium: The impact of a more complex solution medium, organic molecules and zinc ions, J. Cryst. Growth. 553 (2021) 125940.
[9] V. Tazzoli, C. Domeneghetti, The crystal structures of whewellite and weddellite: re-examination and comparison, Am. Mineral. 65 (1980) 327–334.
[10] C. Conti, M. Casati, C. Colombo, E. Possenti, M. Realini, G.D. Gatta, M. Merlini, L. Brambilla, G. Zerbi, Synthesis of calcium oxalate trihydrate: New data by vibrational spectroscopy and synchrotron X-ray diffraction, Spectrochim. Acta - Part A Mol. Biomol. Spectrosc. 150 (2015) 721–730.
[11] I.H. Valido, J.M. Rius-Bartra, R. Boada, M. Resina-Gallego, M. Valiente, M. Lopez-Mesas, Characterization of calcium oxalate hydrates and the transformation process, Chemphyschem. 21 (22) (2020) 2583–2593.
[12] A. Stanković, J. Kontrec, B.N. Džakula, D. Kovačević, B. Marković, D.J. Kralj, Preparation and characterization of calcium oxalate dihydrate seeds suitable for crystal growth kinetic analyses, J. Cryst. Growth. 500 (2018) 91–97.
[13] J.A. Wesson, E.M. Worcester, J.H. Wiessner, N.S. Mandel, J.G. Kleinman, Control of calcium oxalate crystal structure and cell adherence by urinary macromolecules, Kidney Int. 53 (1998) 952–957.
[14] M. Asselman, A. Verhulst, M.E. De Broe, C.F. Verkoelen, Calcium oxalate crystal adherence to hyaluronan-, osteopontin-, and CD44-expressing injured/regenerating tubular epithelial cells in rat kidneys, J. Am. Soc. Nephrol. 14 (12) (2003) 3155–3166.
[15] R. De Bellis, M.P. Piacentini, M.A. Meli, M. Mattioli, M. Menotta, M. Mari, L. Valentini, L. Palomba, D. Desideri, L. Chiarantini, In vitro effects on calcium oxalate crystallization kinetics and crystal morphology of an aqueous extract from *Ceterach officinarum:* Analysis of a potential antilithiatic mechanism, PLoS ONE 14 (6) (2019) e0218734.
[16] K.D. Wood, B.L. Freeman, M.E. Killian, W.S. Lai, D. Assimos, J. Knight, S. Fargue, Effect of alanine supplementation on oxalate synthesis, Biochim. Biophys. Acta - Mol. Basis Dis. 1867 (2021) 165981.
[17] T. Mandal, A.G. Shtukenberg, A.C. Yu, X. Zhong, M.D. Ward, Effect of urinary macromolecules on L-cystine crystal growth and crystal surface adhesion, Cryst. Growth Des. 16 (2016) 423–431.
[18] O.A. Golovanova, V.V. Korolkov, Thermodynamics and kinetics of calcium oxalate crystallization in the presence of amino acids, Crystallogr. Reports. 62 (2017) 787–796.
[19] Y.V. Taranets, I.M. Pritula, O.N. Bezkrovnaya, P.V. Mateychenko, D.S. Sofronov, A.N. Puzan, Effect of charge state of L-aspartic and L-arginine amino acids on morphology of calcium oxalate monohydrate crystals, Cryst. Res. Technol. 53 (2018) 1700133.
[20] A. Vargas-Fernández, M. Sánchez, F. Díaz-Soler, P. Vásquez-Quitral, M. Yazdani-Pedram, A. Neira-Carrillo, Effect of functionalized multiwalled CNTs on the selective formation of calcium oxalate crystals by electrocrystallization, Cryst. Growth Des. 20 (2020) 661–669.
[21] F. Díaz-Soler, C. Rodriguez-Navarro, E. Ruiz-Agudo, A. Neira-Carrillo, stabilization of calcium oxalate precursors during the pre- and post-nucleation stages with poly(acrylic acid), Nanomaterials. 11 (1) (2021) 235.
[22] J. Chi, W. Zhang, C.V. Putnis, L. Wang, Face-specific occlusion of lipid vesicles within calcium oxalate monohydrate, Cryst. Growth Des. 21 (4) (2021) 2398–2404.
[23] M.C. Chauvet, R.L. Ryall, Intracrystalline proteins and calcium oxalate crystal degradation in MDCK II cells, J. Struct. Biol. 151 (2005) 12–17.
[24] A. Gul, P. Rez, Models for protein binding to calcium oxalate surfaces, Urol. Res. 35 (2007) 63–71.
[25] S. Polat, H.B. Eral, Effect of L-alanyl-glycine dipeptide on calcium oxalate crystallization in artificial urine, J. Cryst. Growth. 566–567 (2021) 126176.
[26] S. Farmanesh, J. Chung, D. Chandra, R.D. Sosa, P. Karande, J.D. Rimer, High-throughput platform for design and screening of peptides as inhibitors of calcium oxalate monohydrate crystallization, J. Cryst. Growth. 373 (2013) 13–19.
[27] J.A. Munoz, M. Valiente, Effects of trace metals on the inhibition of calcium oxalate crystallization, Urol. Res. 33 (2005) 267–272.
[28] T.V.R.K. Rao, V.K. Choudhary, Chemoinhibition of mineralization of urinary stone forming minerals by magnesium and zinc ions in aqueous and urinary milieu, Asian J. Chem. 21 (3) (2009) 1730–1738.
[29] B.G. Alamani, J.D. Gale, J.D. Rimer, Zinc ions modify calcium oxalate growth by distinct transformation of crystal surface termination, Cryst. Growth Des. 21 (6) (2021) 3375–3383.
[30] S. Li, W. Tang, M. Li, L. Wang, Y. Yang, J. Gong, Understanding the role of citric acid on the crystallization pathways of calcium oxalate hydrates, Cryst. Growth Des. 19 (6) (2019) 3139–3147.
[31] J.M. Ouyang, L. Duan, B. Tieke, Effects of carboxylic acids on the crystal growth of calcium oxalate nanoparticles in lecithin-water liposome systems, Langmuir. 19 (2003) 8980–8985.
[32] J. Chung, M.G. Taylor, I. Granja, J.R. Asplin, G. Mpourmpakis, J.D. Rimer, Factors differentiating the effectiveness of polyprotic acids as inhibitors of calcium oxalate crystallization in kidney stone disease, Cryst. Growth Des. 18 (9) (2018) 5617–5627.
[33] C.F. Verkoelen, B.G. van Der Boom, J.C. Romijn, Identification of hyaluronan as a crystal-binding molecule at the surface of migrating and proliferating MDCK cells, Kidney Int. 58 (3) (2000) 1045–1054.
[34] C.F. Verkoelen, Crystal Retention in Renal Stone Disease: A Crucial Role for the Glycosaminoglycan Hyaluronan?, J Am. Soc. Nephrol. 17 (2006) 1673–1687.
[35] C.A. Lamontagne, G.E. Plante, M. Grandbois, Characterization of hyaluronic acid interaction with calcium oxalate crystals: implication of crystals faces, pH and citrate, J. Mol. Recognit. 24 (2011) 733–740.

[36] N.W. Poon, M.D.I. Gohel, Urinary glycosaminoglycans and glycoproteins in a calcium oxalate crystallization system, Carbohydr. Res. 347 (2012) 64–68.
[37] T. Ozawa, A new method of analyzing thermogravimetric data, Bull Chem Soc Jpn. 38 (11) (1965) 1881–1886.
[38] J.H. Flynn, L.A. Wall, General treatment of the thermogravimetry of polymers, J. Res. Nat. Bur. Stand. 70 (6) (1966) 487–523.
[39] H.E. Kissinger, Reaction kinetics in differential thermal analysis, Anal. Chem. 29 (11) (1957) 1702–1706.
[40] T. Akahira, T. Sunose, Method of determining activation deterioration constant of electrical insulating materials, Res. Rep. Chiba. Inst. Technol. (Sci Technol) 16 (1971) 22–31.
[41] M. Starink, A new method for the derivation of activation energies from experiments performed at constant heating rate, Thermochim. Acta. 288 (1–2) (1996) 97–104.
[42] W. Tang, Y. Liu, H. Zhang, C. Wan, New approximate formula for Arrhenius temperature integral, Thermochim. Acta. 408 (1–2) (2003) 39–43.
[43] W. Dong, Q. Wu, Dual roles of melamine in the formation of calcium oxalate stones, Cryst. Growth Des. 19 (7) (2019) 3998–4007.
[44] O. Miyake, K. Yoshimura, T. Yoshioka, T. Koide, A. Okuyama, High urinary excretion level of citrate and magnesium in children: Potential etiology for the reduced incidence of pediatric urolithiasis, Urol. Res. 26 (3) (1998) 209–213.
[45] X.Y. Sun, C.Y. Zhang, P. Bhadja, J.M. Ouyang, Preparation, properties, formation mechanisms, and cytotoxicity of calcium oxalate monohydrate with various morphologies, CrystEngComm. 20 (2018) 75–87.
[46] M.T.D. Orlando, L. Kuplich, D.O. de Souza, H. Belich, J.B. Depianti, C.G.P. Orlando, E.F. Medeiros, P.C.M. da Cruz, L.G. Martinez, H.P.S. Corrêa, R. Ortiz, Study of calcium oxalate monohydrate of kidney stones by X-ray diffraction, Powder Diffr. 23 (2) (2008) 59–64.
[47] A. Šter, S. Šafranko, K. Bilić, B. Marković, D. Kralj, The effect of hydrodynamic and thermodynamic factors and the addition of citric acid on the precipitation of calcium oxalate dihydrate, Urolithiasis. 46 (2018) 243–256.
[48] S. Polat, An in vitro evaluation of the effects of *Urtica dioica* and Fructus *Urtica Piluliferae* extracts on the crystallization of calcium oxalate, J. Cryst. Growth. 522 (2019) 92–102.
[49] F. Ibis, P. Dhand, S. Suleymanli, A.E.D.M. Van Der Heijden, H.J.M. Kramer, H.B. Eral, A combined experimental and modelling study on solubility of calcium oxalate monohydrate at physiologically relevant pH and temperatures, Crystals. 10 (2020) 924.
[50] Y.V. Taranets, O.N. Bezkrovnaya, I.M. Pritula, P.V. Mateychenko, L-Threonine amino acid as a promoter of the growth of pathogenic calcium oxalate monohydrate crystals, J. Nanomater. Mol. Nanotechnol. 6 (5) (2017) 1–3.
[51] C. Zhong, Z. Deng, R. Wang, Y. Bai, Inhibition mechanism of calcium oxalate crystal growth by cooperation influence of colloidal selenium nanoparticles and bovine serum albumin, Cryst Growth Des. 15 (2015) 1602–1610.
[52] V. Uskoković, Dynamic light scattering based microelectrophoresis: main prospects and limitations, J. Dispers. Sci. Technol. 33 (12) (2012) 1762–1786.
[53] R.L. Frost, M.L. Weier, Thermal treatment of whewellite - A thermal analysis and Raman spectroscopic study, Thermochim. Acta. 409 (1) (2004) 79–85.
[54] D. Hourlier, Thermal decomposition of calcium oxalate: beyond appearances, J. Therm. Anal. Calorim. 136 (2019) 2221–2229.
[55] R.L. Frost, M.L. Weier, Thermal treatment of weddellite - A Raman and infrared emission spectroscopic study, Thermochim. Acta. 406 (1–2) (2003) 221–232.
[56] Y. Masuda, Y. Ito, R. Ito, K. Iwata, Kinetic study of the thermal dehydration of calcium oxalate monohydrate, Thermochim. Acta. 99 (1986) 205–215.
[57] S. Vyazovkin, Kissinger Method in Kinetics of Materials: Things to Beware and Be Aware of, Molecules. 25 (2020) 2813.
[58] G. Chunxiu, S. Yufang, C. Donghua, Comparative method to evaluate reliable kinetic triplets of thermal decomposition reactions, J. Therm. Anal. Calorim. 76 (2004) 203–216.
[59] H. Eyring, The activated complex in chemical reactions, J. Chem. Phys. 3 (1935) 107–115.
[60] M.G. Evans, M. Polanyi, Some applications of transition state method to calculation of reaction velocities, especially in solution, J. Chem. Soc. Faraday Trans. 31 (1935) 875–894.